Available online at www.sciencedirect.com
ScienceDirect
Remote Sensing of Environment 110 (2007) 216–225
Remote Sensing of Environment
www.elsevier.com/locate/rse

Estimating forage quantity and quality using aerial hyperspectral imagery for northern mixed-grass prairie

Ofer Beeri [a,*], Rebecca Phillips [b], John Hendrickson [b], Albert B. Frank [b], Scott Kronberg [b]

[a] John D. Odegard School of Aerospace Sciences, University of North Dakota, Grand Forks, 58202 ND, United States
[b] USDA-ARS Northern Great Plains Research Lab, United States

Received 29 August 2006; received in revised form 19 February 2007; accepted 23 February 2007

Abstract

Sustainable rangeland stewardship calls for synoptic estimates of rangeland biomass quantity (kg dry matter ha^{-1}) and quality [carbon:nitrogen (C:N) ratio]. These data are needed to support estimates of rangeland crude protein in forage, either by percent (CP_c) or by mass (CP_m). Biomass derived from remote sensing data is often compromised by the presence of both photosynthetically active (PV) and non-photosynthetically active (NPV) vegetation. Here, we explicitly quantify PV and NPV biomass using HyMap hyperspectral imagery. Biomass quality, defined as plant C:N ratio, was also estimated using a previously published algorithm. These independent algorithms for forage quantity and quality (both PV and NPV) were evaluated in two northern mixed-grass prairie ecoregions, one in the Northwestern Glaciated Plains (NGGP) and one in the Northwestern Great Plains (NGP). Total biomass (kg ha^{-1}) and C:N ratios were mapped with 18% and 8% relative error, respectively. Outputs from both models were combined to quantify crude protein (kg ha^{-1}) on a pasture scale. Results suggest synoptic maps of rangeland vegetation mass (both PV and NPV) and quality may be derived from hyperspectral aerial imagery with greater than 80% accuracy.
© 2007 Elsevier Inc. All rights reserved.

Keywords: HyMap; Rangeland; Biomass; Carbon; Nitrogen ratio; Crude protein

1. Introduction

The 124 million ha of northern U.S. mixed-grass prairie rangelands (Vogelmann et al., 2001) are typically managed as 20 to 200-ha pastures, calling for synoptic decision support tools at high to moderate spatial resolutions. Rangeland managers need reliable, current data delineating vegetation quantity and quality across multiple landscapes to support management strategies (Moran et al., 1997). Remote sensing-based products could assist with rangeland carrying capacity assessment (Hunt et al., 2003), for range condition varies widely with climate and land use. While synoptic data indicative of range condition are needed, remote assessment products rarely provide information in physically meaningful units, e.g. kg ha^{-1}. Remote sensing-based model formulation is often based on data from one image or one area of interest, so extrapolation one area could be spatially limited. Here, we take steps to address these issues by developing and validating spectral models for rangeland biomass (live only and total) and C:N ratio to calculate crude protein by mass (CP_m) on a pasture scale using two images acquired on the same day over neighboring ecoregions (Fig. 1).

Spectral estimates of rangeland biomass (kg ha^{-1}) at high to moderate spatial resolutions are needed to delineate variability for pastures within the larger northern mixed-grass prairie region. Spectral signatures are influenced by variable landscape factors such as plant community distribution (Boelman et al., 2005), soil color (Gao et al., 2000), hydrology (Todd & Hoffer, 1998), and topography (Kawamura et al., 2005). Consequently, spectral algorithms should be developed at scales that encompass these factors without compromising spatial resolution within and among pastures. Many studies correlate spectra with relative differences in biomass (Everitt et al., 1989; Frank & Aase, 1994; Rundquist, 2002; Tucker et al., 1983), yet few delineate the amount of plant material on a mass per unit area basis (kg ha^{-1}). A spectral model for estimating biomass based on data for more than one mixed-grass prairie ecoregion would

* Corresponding author. Tel.: +1 701 777 6095; fax: +1 701 777 3711.
E-mail address: beeri@aero.und.edu (O. Beeri).

0034-4257/$ - see front matter © 2007 Elsevier Inc. All rights reserved.
doi:10.1016/j.rse.2007.02.027

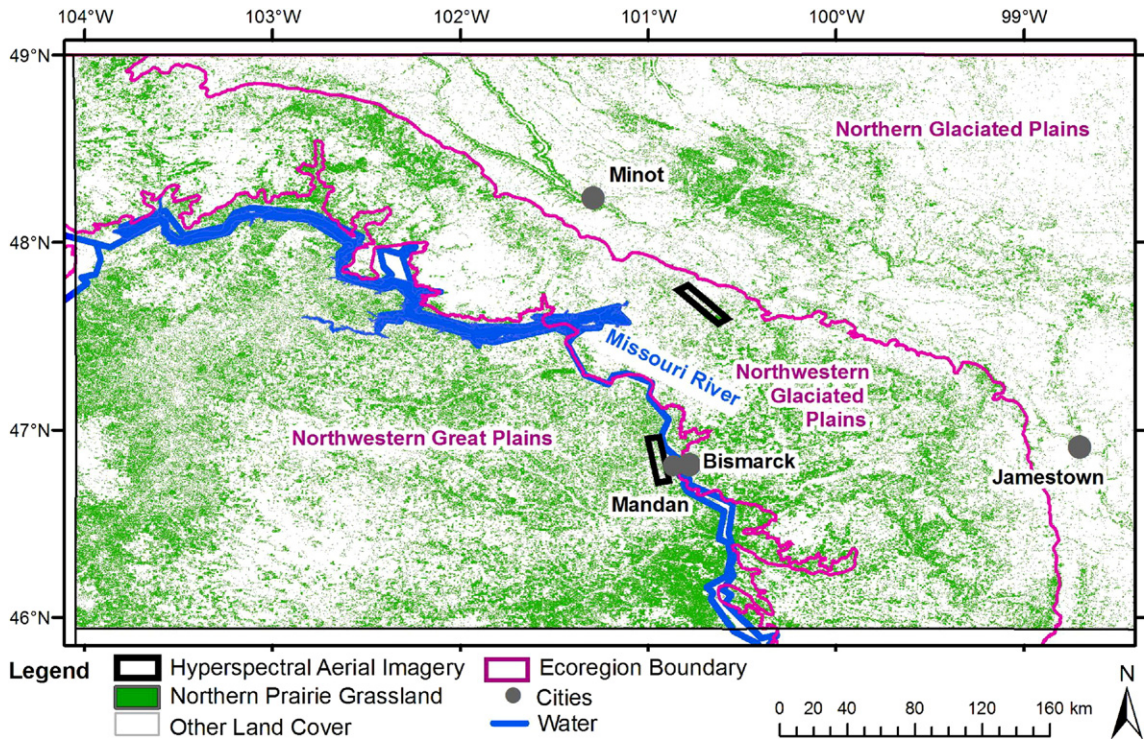

Fig. 1. North Dakota northern prairie grasslands mapped by Strong et al. (2005) and United States ecoregions mapped by Omernik (1987).

likely reduce site specificity by including a large breadth of geospatial variability.

Canopies comprised of photosynthetically active (PV) and non-photosynthetically active (NPV) vegetation are ubiquitous in northern mixed-grass rangelands, thereby affecting vegetation quality and spectral response. NPV interferes with plant biomass–spectra relationship when using handheld instruments (Frank & Aase, 1994; Rundquist, 2002) and when scaling up from handheld to aerial and satellite-borne sensors (Loris & Gianelle, 2006; Serrano et al., 2002). Despite issues associated with NPV, both PV and NPV contribute to biogeochemical cycling, which is an essential component to ecosystem functional assessment. Consequently, inclusion of both pools in remote sensing product development is necessary.

Remote rangeland assessment tools for vegetation quality on a mass basis are lacking. Vegetation quality is commonly expressed in terms of percent crude protein [CP_c (mg g^{-1})], or nitrogen [N_c (mg g^{-1})], which is a factor in animal management. Crude protein (CP_c) or N_c has been correlated with spectra using handheld sensors for grasses (Mutanga et al., 2004; Starks et al., 2006) and airborne sensors for forests (Matson et al., 1994; Wessman et al., 1988). However, leaf moisture masks leaf N_c spectral signature in fresh vegetation (Kokaly & Clark, 1999), which presents a problem with quantification of forage quality under variable drought stress. This has been addressed using hyperspectral data manipulation, such as continuum removal (CR) (Curran et al., 1992; Kokaly & Clark, 1999), and by experimentally separating effects of leaf moisture from leaf quality using C:N ratio (Phillips et al., 2006). Methods to remotely estimate range condition are available (Hunt et al., 2003), although methods to remotely and independently assess forage quality and quantity are lacking for northern mixed-grass prairie.

This manuscript describes how we i) developed and validated spectral algorithms for estimating rangeland biomass using HyMap imagery acquired over two Northern Plains ecoregions, ii) applied and validated a previously published algorithm for forage quality (C:N ratio) on the HyMap airborne sensor, and iii) combined biomass and C: N ratio estimates to map the mass of crude protein (CP_m) on a pasture scale.

2. Methods

2.1. Image acquisition areas-of-interest (AOI)

Aerial hyperspectral images were acquired for two areas-of-interest (AOIs), 13,250 ha each, located on opposite sides of the Missouri River near the center of North Dakota (Fig. 1). The northeast AOI in Fig. 1 is located in the Northwestern Glaciated Plains (NGGP) ecoregion (Omernik, 1987), where kettle holes, kames, and moraines are common among gently rolling continental glacial till plains. Natural prairie vegetation is characterized by western wheatgrass [*Pascopyrum smithii* (Rydb.) A. Löve], needle-and-thread [*Hesperostipa comata* (Trin. and Rupr.) Barkworth], green needlegrass [*Nassella viridula* (Trin.) Barkworth], and blue grama associations [*Bouteloua gracilis* (Willd. ex Kunth) Lag. ex Griffiths] (USDA, 2006). The southwest AOI in Fig. 1 is located in the Northwestern Great Plains (NGP) ecoregion (Omernik, 1987), with gently rolling continental glacial till plains and rolling hills. Natural prairie vegetation is characterized by grama–needlegrass–wheatgrass associations. Similar to the NGGP

ecoregion, native species common to this area are blue grama, green needlegrass, needle-and-thread, and western wheatgrass (USDA, 2006). Introduced graminoid species common to the both ecoregions include Kentucky bluegrass [*Poa pratensis* L.] and crested wheatgrass [*Agropyron desertorum* (Fisch. ex Link) J.A. Schultes], which have invaded large areas of native rangeland in recent decades.

Land use for both areas is predominately agricultural, with 50% in annual crop production and 20–30% in native range and grass production. The remaining 20–30% of land area is covered by wetlands, shrub–woodlands, and anthropogenic structures (Phillips et al., 2005; Strong et al., 2005), which is similar to state-wide land use patterns (Strong et al., 2005). Weather stations at Turtle Lake (47°31′N, 100°54′W; located within the NGGP AOI) and Mandan (46°49′N, 100°55′W; located within the NGP AOI) recorded an annual average of 434 and 442 mm of rainfall and 78 and 80 mm of precipitation as snowfall, respectively, over the last 30 years. In 2005, total rainfall was 490 mm for both Turtle Lake and Mandan weather stations. Precipitation as snowfall in 2005 was twice as high in Turtle Lake (60 mm) as compared to Mandan (31 mm).

2.2. Vegetation field measurements

Two moderately grazed pastures (areas >250 ha) and comprised of graminoids, sedges, and forbs were selected within each image acquisition AOI for spectral model development and validation. Soils beneath pastures in the NGGP AOI are classified as Max–Zahl loams (frigid, typic haplustoll–calciustoll). Soils beneath pastures in the NGP AOI are classified as Zahl–Williams loams (frigid, typic calciustoll–argiustoll). To assess if pastures were representative of the NGGP and NGP ecoregions, we determined canopy cover by species using the Daubenmire method. Specifically, we used 0.1 m^2 quadrats placed every 2-m along 30-m transects for each pasture. Canopy cover was measured on Aug 29 2005 for pastures in the NGGP AOI and on July 5 2005 for pastures in the NGP AOI. Canopies are typically fully developed by early July; however, in 2005, spring drought was following by unusually high rainfall during July and August. Consequently, maximum canopy cover was delayed until August.

Within each one of the four pastures, we randomly selected four points using the ERDAS Imagine 8.7 software (Leica Geosystems GIS and Mapping LLC, Norcross, GA) randomization procedure and mapped 10 × 10 m plots around each point using a sub-meter, real-time differential Trimble Geo XT GPS Beacon receiver with an external antenna (Trimble Navigation, Sunnyvale, CA). We chose this plot size (100 m^2) because we expected the HyMap data to be acquired as < 10 m pixels. Remote sensing-based data acquired from the HyMap sensor were collected from these points. To determine biomass representative of each 100 m^2 plot, we collected vegetation data from two strips adjacent to each point (Fig. 2). We clipped strips of vegetation (1 × 10 m) located 2-m to the east and 2-m to the west of each point to ground level on August 29 and 30, 2005. Additionally, we clipped two small (0.25 m^2) quadrats located 1-m to the east and 1-m to the west of each point. Vegetation from each quadrat were separated into standing live (PV), standing dead (NPV), and detrital plant material lying on the surface (NPV). The proportion of PV and NPV identified in each small quadrat was used to estimate amount of PV and NPV in the larger strip. Dry mass for samples collected from strips and quadrats was determined after samples were oven-dried at 60 °C for 48 h. Plot averages (both strips) for PV and NPV were used for comparison with spectra collected at each plot center point (Fig. 2).

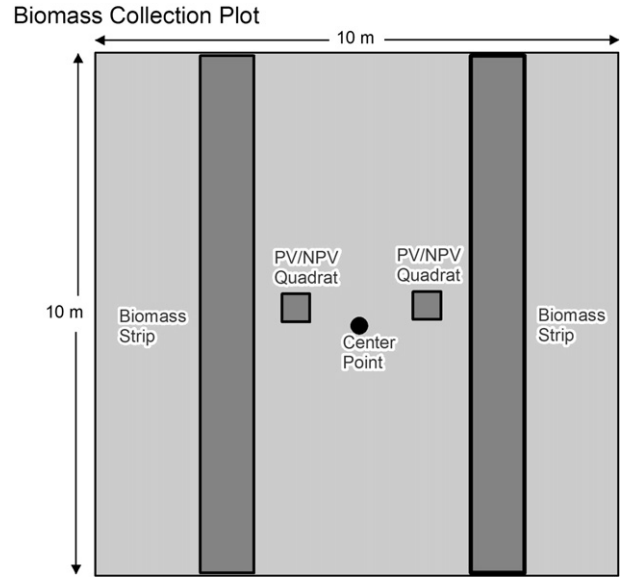

Fig. 2. Biomass samples collected for each 10 × 10 m plot.

Separated, dried materials were then ground (1 mm mesh) and analyzed for carbon content (C_c) and N_c by dry combustion with an Elementar Vario MAXCNS (Elementar Americas, Mt. Laurel, NJ). Spectral data were converted to PV biomass [PV_DM (kg ha^{-1})] and total biomass [All_DM (kg ha^{-1})] by regressing spectra on dry mass calculated for each plot. Canopy C and N (kg ha^{-1}) and C:N ratios were calculated for each plot by weighting the mass of C_c and N_c for PV and NPV pools. We separately tested for differences in All_DM, PV_DM, and C:N ratio among pastures and between ecoregion AOIs using a hierarchal mixed model in SAS (v. 9.1), which included the random effect of pasture nested inside AOI (Littell et al., 1996).

Spectra were recorded for clipped and separated vegetation in the field on July 11, 2005 using a Fieldspec Pro-FR ® spectroradiometer (Analytical Spectral Devices, Boulder, CO), which detects light in the 350–2500 nm wavelength range and records light as radiance, Watts per square meter per steradian per nanometer (W m^{-2} sr^{-1} nm^{-1}). Prior to recording spectra, the spectroradiometer was calibrated to a spectralon target (Labsphere, Inc. North Sutton, NH). Each observation was comprised of one Spectralon record, five target surface records, then one Spectralon record. We calculated observation target reflectance (multiplied by 10,000 for storage efficiency) using the formula:

$$R_\lambda = 10,000 \times \left(\left(\sum_1^n T_\lambda\right)/n\right) / \left(\left(\sum_1^2 S_\lambda\right)/2\right) \quad (1)$$

R_λ is the reflectance for each wavelength, T_λ is the target radiance, n is the target measurements and S_λ is the Spectralon radiance. These spectra were plotted to qualitatively evaluate the effect of PV and NPV on spectral reflectance (Fig. 3).

2.3. Hyperspectral data processing

Two hyperspectral images were acquired for our study landscapes by the HyMap sensor, operated by HyVista Corporation (http://www.hyvista.com/main.html). HyMap uses four different detectors to cover spectra from 450–2480 nm. Bandwidths ranged from 13 to 20 nm for a total of 126 bands (Cocks et al., 1998). HyMap was flown at noon local time, 29th August 2005 at 4800 and 4750 m above sea level with flight azimuth at 141° and 170°, for the NGGP and NGP AOIs, respectively. HyVista supplied data that were geo-referenced to UTM Zone 14, Datum WGS 84, 16-bit, and calibrated to ground reflectance. Pixel size varied from 7.6 m in the NGGP AOI to 8.7 m in the NGP AOI. Dataset accuracy and quality were evaluated for each image individually using the following procedures. To evaluate geo-location, HyMap data were compared with 1-meter, digital Ortho-mosaic images (USDA-FSA-APFO). We found geo-location root–mean–square-error (RMSE, Eq. (13)) was smaller than one-half pixel. To evaluate Signal-to-Noise ratio (SNR), spectra were collected from uniform areas within each image. The SNRs for wavelengths <480, 1390–1435, 1953–1991 and >2480 nm were near zero and thus eliminated from the dataset, with 114 bands remaining. Further, "Smile" phenomena (Datt et al., 2003; Schlerf et al., 2005) are known hyperspectral imagery problems that refer to systematic increases in the pixel values from the sun direction or from the image center. We verified imagery homogeneity for all bands using spectral signatures from roads that cross each image. Data were atmospherically corrected by HyVista Corp using atmospheric and solar radiation profile information recorded during the flight (Cocks et al., 1998). We confirmed that image reflectance values were similar to ground-based reflectance values recorded at 19 uniform areas (>1 ha) on the day of the flight (between 1100 and 1400 h) using a handheld spectroradiometer (Clark et al., 2002; Liang et al., 2002). Calculated RMSEs for the visible bands were <0.020 and RMSEs for the infrared bands were <0.035.

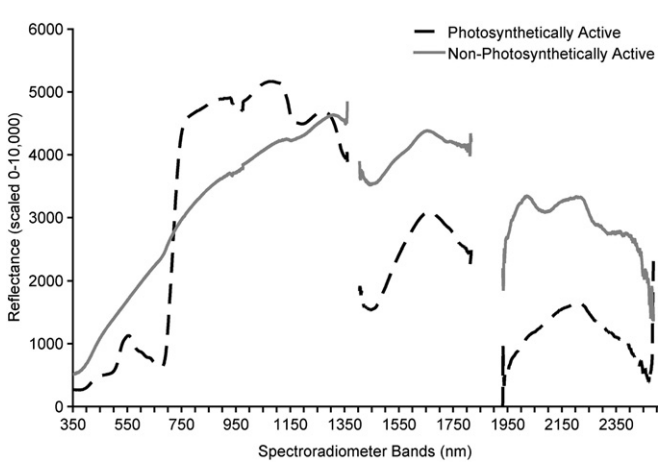

Fig. 3. Spectral signatures for photosynthetically and non-photosynthetically active vegetation recorded using a handheld spectroradiometer (ASD Inc. Denver, CO).

2.4. Hyperspectral algorithm development and validation

Four of the eight biomass plots within each image acquisition AOI were randomly selected for use in algorithm development; remaining plots were used for validation. HyMap spectra (114 bands) were extracted from the center of each plot for comparison with field biomass data. We identified bands most responsive to changes in biomass (PV and ALL) separately for each landscape by calculating the covariance, or the simultaneous deviations of biomass and spectra from their means, for each of the 114 bands.

Bands with the highest covariance for PV_DM and All_DM were similar for each image, with highest values found for a range of 22 continuous bands centered between 991 and 1306 nm. Since bands with highest covariance were the same for both landscapes, data were combined for further analyses. Band 48, centered at 1139 nm, covaried most strongly with biomass. The 22 bands from 991 to 1306 nm were used as input for spectra continuum removal (CR) and summed for the entire CR area (Fig. 4). We defined these end points for the CR line (Kokaly, 2001) because these related most strongly to our variable of interest (Kokaly & Clark, 1999) rather than performing CR on the entire spectrum (Huang et al., 2004). By aggregating those bands most responsive to total biomass, slight differences in spectral response to mixed PV and NPV biomass are expanded for greater spectral resolution (Clark, 1999). We utilize the area below the original reflectance and above the CR line (Kokaly, 2001), compared with isolating areas above the original reflectance and below the CR line only (Kokaly & Clark, 1999).

To establish the CR, we calculated the continuum line as new reflectance values for each band:

$$R'_{\mathrm{Bx}} = \left(\left(\frac{R_{\mathrm{B991}} - R_{\mathrm{B1306}}}{n-1}\right)^{*}\mathrm{Bx}_{(n-1)}\right) + R_{\mathrm{B991}} \tag{2}$$

where R'_{Bx} is the CR reflectance value for each band, R_{B991} and R_{B1306} are the end-point bands reflectance values, n is the number of bands in the analysis, and Bx is the center location of the $n-1$ band. This means the first band will have location zero while the second band will have location 1.

We then calculated CR by band depth normalization in order to minimize topographic and atmospheric affects. Results were summed for each band to represent the CR area (Kokaly & Clark, 1999):

$$\mathrm{CR}_{\mathrm{B991-B1306}} = \sum_{\mathrm{B991}}^{\mathrm{B1306}} \left(\frac{1 - R'/R}{1 - R_{\mathrm{h-pca}}'/R_{\mathrm{h-pca}}}\right) \tag{3}$$

$\mathrm{CR}_{\mathrm{B991-B1306}}$ represents the accumulated CR for bands between 991 to 1306 nm, R' the $\mathrm{CR}_{\mathrm{B991-B1306}}$ reflectance, and R the original reflectance. $R'_{\mathrm{h\text{-}pca}}$ and $R_{\mathrm{h\text{-}pca}}$ are the $\mathrm{CR}_{\mathrm{B991-B1306}}$

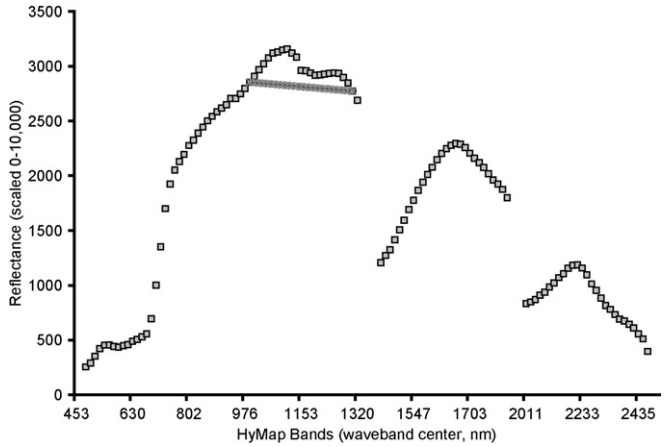

Fig. 4. Hyperspectral data recorded by HyMap over rangeland plots. Continuum removal was preformed on bands centered from 991 to 1306 nm.

reflectance and the original reflectance values for the band centered at 1139 nm.

NDVI was also calculated as broad band (bNDVI) and narrow band (nNDVI) indices to evaluate accuracy for both (Elvidge & Chen, 1995):

$$\mathrm{bNDVI} = \frac{B4 - B3}{B4 + B3} \tag{4}$$

$$\mathrm{nNDVI} = \frac{B802 - B673}{B802 + B673} \tag{5}$$

B4 and B3 correspond to Landsat 5 bands 4 (623–695 nm) and 3 (781–906 nm) as convolved from the HyMap bands (Jacquemoud et al., 1995), while B802 and B673 are the bands centered at 802 and 673 nm, respectively.

To estimate biomass for each pixel, bNDVI, nNDVI, and $\mathrm{CR}_{\mathrm{B991-B1306}}$ spectral values collected from the HyMap imagery were regressed separately on 1) all measured biomass, including PV and NPV vegetation (All_DM)] and 2) PV vegetation only (PV_DM) (Fig. 5).

$$\mathrm{All_DM}_1 = 1114.5 \times (\mathrm{CR}_{\mathrm{B991-B1306}}) - 10074 \tag{6}$$

$$\mathrm{All_DM}_2 = 26769 \times (\mathrm{nNDVI}) - 9176.79 \tag{7}$$

$$\mathrm{All_DM}_3 = 29338 \times (\mathrm{bNDVI}) - 11037 \tag{8}$$

$$\mathrm{PV_DM}_1 = 381.03 \times (\mathrm{CR}_{\mathrm{B991-B1306}}) - 2767.7 \tag{9}$$

$$\mathrm{PV_DM}_2 = 8498.5 \times (\mathrm{nNDVI}) - 2111.5 \tag{10}$$

$$\mathrm{PV_DM}_3 = 9358.8 \times (\mathrm{bNDVI}) - 2726.6. \tag{11}$$

In addition, we estimated the C:N ratio with the Rangeland C:N Formula (Phillips et al., 2006), which utilizes mid-infrared and red spectral regions:

$$\mathrm{C:N} = 2.62 + 56.35 \times \left(1 - \frac{((B1653 + B1666) - (B673 + B688))}{((B1653 + B1666) + (B673 + B688))}\right) \tag{12}$$

B1653, B1666, B673 and B688 represent bands centered at 1653, 1666, 673 and 688 nm, respectively.

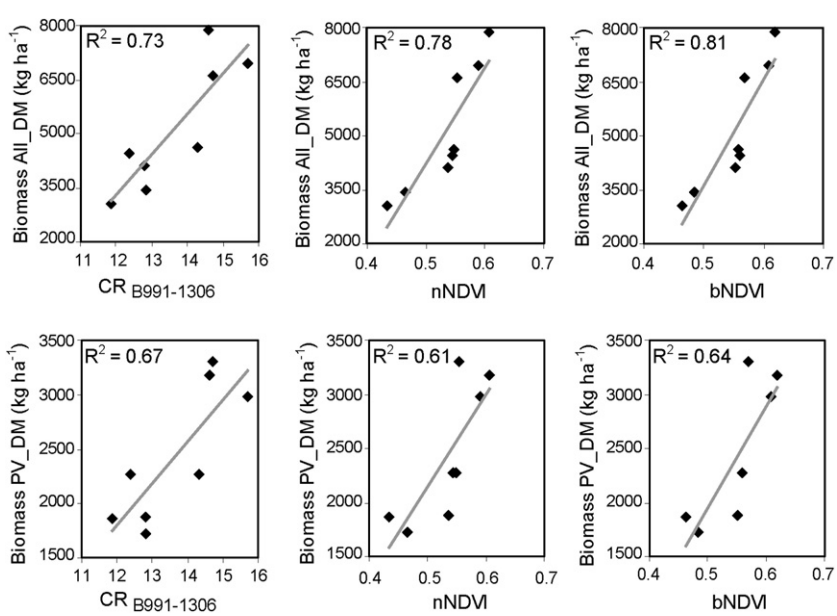

Fig. 5. Scatter plots of measured biomass and $\mathrm{CR}_{\mathrm{B991-B306}}$, nDNVI and bDNVI. All regression analyses were statistically significant ($p < 0.05$).

Table 1
Canopy cover (%) by species measured for pastures within each image acquisition AOI in the Northern Glaciated Great Plains and Northern Great Plains ecoregions

Plant ID	Type	NGGP AOI % canopy cover	NGP AOI % canopy cover
Achillea L.	F	0.94	
Agropyron desertorum (Fisch. ex Link) J.A. Schultes	G		11.70
Anemone canadensis L.	F	0.56	
Amorpha L.	F	0.56	
Antennaria Gaertn.	F		0.50
Aristida L.	G		0.33
Artemisia campestris L.	F	0.56	0.17
Artemisia frigida Willd.	F		0.20
Artemisia vulgaris L.	F		0.4
Aster L.	F	3.25	
Bouteloua dactyloides (Nutt.) J.T. Columbus	G		0.07
Bouteloua gracilis (Willd. ex Kunth) Lag. ex Griffiths	G	11.38	15.83
Brassica L.	F		1.67
Bromus inermis Leyss.	G		1.0
Calystegia R. Br.	F		0.73
Carex L.	S	12.18	5.83
Chaetadelpha Gray ex S. Wats.	F	0.13	
Cirsium P. Mill.	F	0.88	0.33
Cirsium undulatum (Nutt.) Spreng.	F	0.06	
Comandra Nutt.	F		0.83
Echinacea Moench	F	1.55	
Elymus caninus (L.) L.	G	0.56	
Euphorbia esula L.	F		0.67
Grindelia squarrosa (Pursh) Dunal	F		1.0
Grindelia Willd.	F	0.38	0.5
Gutierrezia sarothrae (Pursh) Britt. and Rusby	F	0.19	
Hesperostipa comata (Trin. and Rupr.) Barkworth	G	3.94	
Hesperostipa curtiseta (A.S. Hitchc.) Barkworth	G	0.38	
Koeleria Pers.	G	0.38	0.07
Lactuca tatarica (L.) C.A. Mey.	F	0.13	
Liatris Gaertn. ex Schreb.	F	0.88	
Linum rigidum Pursh	F	0.25	
Medicago L.	F		0.17
Medicago lupulina L.	F	0.13	
Melilotus officinalis (L.) Lam.	F	2.00	0.3
Melilotus P. Mill.	F	4.25	
Muhlenbergia cuspidata (Torr. ex Hook.) Rydb.	G	1.63	
Nassella viridula (Trin.) Barkworth	G	13.38	2.0
Pascopyrum smithii (Rydb.) A. Löve	G	6.64	7.63
Phlox L.	F	0.06	
Poa pratensis L.	G	25.93	20.17
Polygala alba Nutt.	F	0.88	
Psoralidium Rydb.	F	0.75	
Ratibida Raf.	F		0.1
Schizachyrium Nees	F		
Solidago L.	F	0.50	0.67
Sorghastrum Nash	G	0.25	
Sphaeralcea coccinea (Nutt.) Rydb.	F		0.67
Taraxacum G.H. Weber ex Wiggers	F	0.13	0.83
Tragopogon L.	F	0.38	
Vernonia Schreb.	F		0.17
Vicia americana Muhl. ex Willd.	F		0.27
Vicia hyrcanica Fisch. and Mey.	F	0.05	
Unknown forb	F	0.15	
Unknown grass	G	0.85	0.05
Open canopy		2.90	25.14

Types F, G, and S represent forb, graminoid, and sedge life-forms, respectively.

Biomass estimates using Eqs. (6)–(11) were compared with ground data reserved for validation. C:N ratio data, based on a previously published algorithm, were compared with the 16 plots. RMSE and relative error (RE) were calculated:

$$\mathrm{RMSE} = \sqrt{\frac{\sum_{i}^{n} (M_i - E_i)^2}{n}} \tag{13}$$

$$\mathrm{RE} = \frac{\sum_{i}^{n} (\mathrm{Absolute}(M_i - E_i)/M_i)}{n} \tag{14}$$

M_i represents measured and E_i represents estimated values for each plot i, while n is the number of plots.

We used All_DM and C:N ratio to calculate $\mathrm{CP_m}$ by first converting C:N ratio to $\mathrm{N_c}$ and then $\mathrm{CP_c}$ using constants for grassland $\mathrm{C_c}$ (400 mg $\mathrm{g^{-1}}$) and for conversion of $\mathrm{N_c}$ to crude protein (0.0625).

$$\mathrm{CP_c} = 0.0625 \times 100 \times \left(\frac{400}{\mathrm{C:N\ ratio}}\right) \tag{15}$$

$$\mathrm{CP_m} = \frac{\mathrm{CP_c}}{1000} \times (\mathrm{All_DM}). \tag{16}$$

To demonstrate application of these spectral models, data for a known pasture located in the NGP AOI were mapped using the HyMap image. We report pasture-scale averages for total biomass (All_DM), photosynthetically active vegetation only (PV_DM), C:N ratio, and crude protein in total biomass $\mathrm{CP_m}$.

3. Results and discussion

3.1. Field measurements

Graminoids found in both NGGP and NGP AOIs included green needlegrass, needle-and-thread, blue grama, western wheatgrass, crested wheatgrass, and Kentucky bluegrass (Table 1). Most of the dominant species found at our field plots are typical native and introduced species for these ecoregions (USDA, 2006). Graminoids dominated the plant canopy in the NGP AOI pastures (Table 1), comprising over

Table 2
Pasture biomass data collected from NGGP and NGP ecoregion AOIs, including average, standard deviation, and the percent of total biomass by mass for standing live, standing dead, and detrital pools

AOI	Standing live (kg ha^{-1})			Standing dead (kg ha^{-1})			Detritus (kg ha^{-1})			All_DM (kg ha^{-1})	
	Mean	S.D.	Percent of total (All_DM)	Mean	S.D.	Percent of total (All_DM)	Mean	S.D.	Percent of total (All_DM)	Mean	S.D.
NGGP	2408	727	50%	1330	368	28%	1062	368	22%	4799	1399
NGP	2398	688	44%	1490	622	28%	1506	893	28%	5394	2125

60% of total plant cover. The graminoid versus forb distribution was more uniform in the NGGP AOI. In both ecoregions, forbs were represented by small proportions for a variety of species (Table 1), with 10–20 different forbs per pasture. Total vegetative cover (not rocks, litter, or soil) measured on August 29 for pastures in the NGGP AOI were over 95%. Vegetative cover measured for pastures in the NGP AOI on July 5 were sparser than usual (75%). This condition likely changed following high July–August rainfall (179 mm), but August cover data are not available.

Biomass measured at the end of August were similar among plots for total biomass (All_DM), PV biomass (PV_DM), and C:N ratio (Table 2). Since differences between AOIs were not significant for any of these variables ($p>0.05$), data for both images were combined for subsequent analyses. All_DM ranged from 3100 to 7900 kg ha^{-1}, for an average of 5180 kg ha^{-1} (+/−1890). PV_DM comprised 44 to 60% of the total mass for all plots, for an average of 2410 kg ha^{-1} (+/−680). C_c for both PV and NPV pools were similar, with an overall average of 401 mg g^{-1} (+/−12), which is near the 400 mg g^{-1} value commonly found for northern mixed-grass prairie rangeland. Average C:N ratio measured for PV vegetation was 31.0, compared with 39.0 for NPV (standing and detrital pools). When weighted by mass for each pool, plot C:N values ranged from 25.3 to 38.3.

3.2. Spectral biomass estimates

We compared biomass estimates [Eqs. (6)–(11)] with plot data reserved for accuracy assessment (Table 3)). The $CR_{B991-B1306}$-based algorithms for All_DM1 and for PV_DM [Eqs. (6) and (9) respectively] more closely tracked ground data than algorithms based on NDVI (Fig. 6A,B). In general, algorithms using NDVI tended to overestimate biomass, as compared with algorithms using $CR_{B991-B1306}$. Accuracy assessments for All_DM and PV_DM derived from multispectral (bNDVI) were comparable to those derived from hyperspectral (nNDVI) for the same sensor. Overall, the lowest relative error for biomass was found using the $CR_{B991-B1306}$-based algorithm [Eq. (6)]. Since mean measured biomass was 5180 kg ha^{-1}, the $CR_{B991-B1306}$ RMSE for All_DM1 (976 kg ha^{-1}) represents 19% of the mean. This error is comparable to other satellite-based grassland estimates, where RMSEs reported (6.7 to12.2 kg ha^{-1}) represented 25% of the mean (33.7 to 42.0 kg ha^{-1}) in Australia (Hill et al., 2004).

Greatest covariance between biomass and spectra were found for the 991 to 1306 nm spectral region, so the $CR_{B991-B1306}$-based algorithm more closely approximated rangeland biomass than the bNDVI-and nNDVI-based algorithms. The $CR_{B991-B1306}$ spectral region is not common among current, moderate-to-high resolution satellites; however the utility of this region is suggestive for future sensor design. Both PV and NPV biomass estimates were accurate to within 18% of measured values. Over 50% of measured rangeland biomass consisted of NPV vegetation (Table 2), which tends to mask spectral responses in the red (~680 nm) and NIR (~800 nm) regions (Fig. 3). Consequently, spectral algorithms using only the red and NIR regions (such as NDVI) are less accurate as the proportion of NPV increases.

Relative errors for PV estimates were 0.21, 0.23, and 0.22 using the $CR_{B991-B1306}$-, nNDVI-, and bNDVI-based formulae, respectively. The close range in accuracy among formulae for PV suggests that spectral estimates may not improve with narrow-band data, given similar spatial resolution. The RMSE for PV using bNDVI was 547 kg ha^{-1}, which is lower than the standard deviation (680 kg ha^{-1}) for live biomass measured. The presence of NPV likely contributed to estimate error, for NPV is ubiquitous in this region (Frank & Aase, 1994). PV is regularly mapped using parameters such as Leaf Area Index (Asrar et al., 1984; Curran, 1983; Myneni et al., 2002), which is often correlated with biomass. Here, we estimate PV in units of mass per area. Overall, quantification of both PV and NPV provide not only the amount of live material, but also the total amount of vegetation potentially available to micro- and macro-scale grazers.

3.3. C:N ratio spectral estimates

Average estimated C:N ratio (31.4+/−0.9) was similar to average measured C:N ratio (31.6+/−3.7) with an RMSE of 3.4 and a relative error of 0.081 (Fig. 6C). This error very closely approximates error reported for the same formula on Landsat and ASTER sensors (Phillips et al., 2006). Results are similar to errors associated with plant N estimates using hyperspectral

Table 3
Accuracy assessment results for estimated total biomass (All_DM) and live biomass (PV_DM) following application of three indices

Formula	Index	RMSE (kg ha^{-1})	Relative error
All_DM1	$CR_{B991-B1306}$	976	0.175
All_DM2	nNDVI	1447	0.265
All_DM3	bNDVI	1403	0.257
PV_DM1	$CR_{B991-B1306}$	473	0.211
PV_DM2	nNDVI	558	0.231
PV_DM3	bNDVI	547	0.223

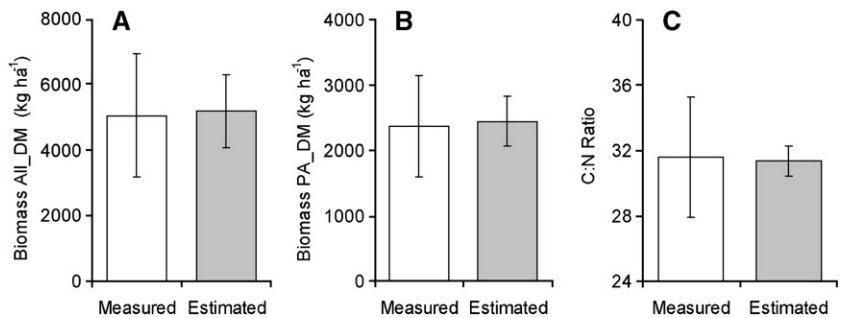

Fig. 6. Measured and estimated biomass and C:N ratio for validation plots using Eqs. (6), (9), and (12). Inset A depicts total biomass (All_DM) includes photosynthetically active (PV), non-photosynthetic active (NPV), and detrital (NPV) pools, while inset B depicts estimated and actual values for PV vegetation only. Inset C depict C:N ratio for all aboveground forage (all PV and NPV vegetation).

data recorded from handheld platforms (Kokaly and Clark, 1999; Mutanga et al., 2004).

C:N ratio is a measure of canopy forage quality that incorporates both PV and NPV vegetation, and C:N ratio spectral estimates were accurate for both AOIs to within 8%. Grazing animals rely on high protein vegetation with low C:N ratios (<36). Given C:N ratio, crude protein is easily estimated for northern mixed-grass prairie. These are useful data for rangeland managers who need to know when pastures can no longer meet minimum animal maintenance requirements (~70 mg g^{-1} crude protein, depending upon the animal). Annual or inter-annual maps of pasture forage quality can help guide decision makers to understand how rangelands vary spatially and temporarily. As vegetation quality changes, so do vegetative decomposition rates (Enriquez et al., 1993). Consequently, remotely-derived estimates for C:N ratio across ecoregions, as demonstrated by application of published algorithm at different ecoregions, can serve as geo-referenced input to spatially explicit ecological models.

Estimated biomass, C:N ratio, and crude protein mapped for a known pasture (Fig. 7) illustrate a potential rangeland management application. Pasture 23, depicted in Fig. 7, is similar vegetatively to the previously described field plots (data not shown). The entire pasture is comprised of 1574 HyMap pixels. We calculated average total biomass (4600+/−970 kg ha^{-1}), C:N ratio (32+/−1), and crude protein of (360+/−80 kg ha^{-1}). However, only one-half of the total biomass was photosynthetically active (average PV=2300+/−330 kg ha^{-1}). Since animals preferentially select PV, the mass of PV is also important when considering animal stocking rates. Further work is needed, not only for additional spectral model validation, but also research that integrates remote estimates

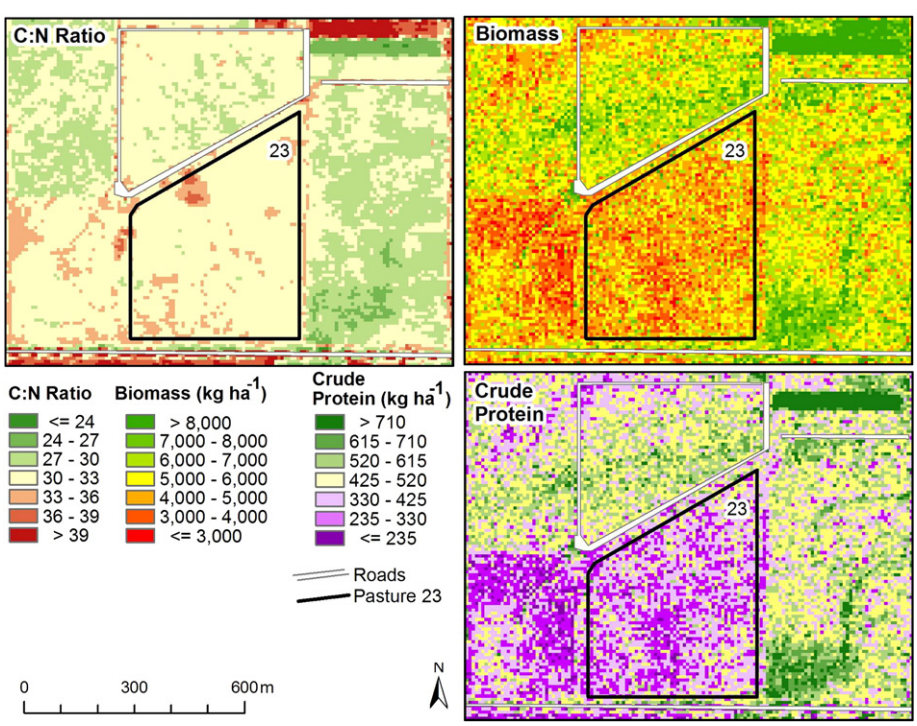

Fig. 7. Forage quality (C:N ratio), forage quantity (All_DM), and crude protein quantity (CP_m) for pastures located at the USDA-ARS Northern Great Plains Research Lab in Mandan, ND (46°46′N, 100°55′W). Maps for each variable were derived from application of algorithms for C:N ratio, All_DM, and CP_m on HyMap sensor data acquired August 29, 2005 [see text, Eqs. (6), (12), (14)].

with the large herbivores relying on these pastures. Experiments that integrate remote sensing with vegetation removal by large herbivores could be designed to determine the utility of these data by tracking estimated crude protein versus animal weight gains. Connection of the animal unit with terrestrial remote sensing may represent the next level necessary for practical remote sensing applications.

4. Conclusions

Many environmental questions require quantitative analyses of range condition, and research is limited by relying on knowledge acquired only at plot scales or for site-specific pastures only (Roughgarden et al., 1991). Development and validation of algorithms using more than one ecoregion and AOI reduces site-specificity issues and provides a foundation for broader spatial application. Application of remote sensing products by rangeland managers and global change scientists require that they be field-tested and errors identified. We assessed rangeland condition on a pasture-by-pasture basis, as measured by forage quality and quantity, and found results were accurate across two ecoregion AOIs with 8% and 18% error, respectively. These initial results are promising but further validation is needed to assess accuracy when these methods are extrapolated to regional scales. Given 10-m spatial resolution and spectral reflectance in the 670–690 and 1650–1670 and 990–1300 nm regions, we demonstrate how quantification of rangeland biomass and quality (C:N ratio) at pasture scales may be achieved. Results indicate remote sensing-based observations will facilitate large-scale hypothesis testing necessary for scaling up our understanding of rangeland condition from field plots to ecoregions.

Acknowledgment

We would like to thank Scott Bylin, Clay Erickson, Gordon Jensen, and Mary Kay Tokach for their help with collection and identification of grasses. We are grateful to Susan Moran, Ray Hunt, and Roger Clark for their insightful comments and editorial reviews. This work was supported by USDA Cooperative Agreement 58-5445-3-314, the U.S. Environmental Protection Agency Wetland Protection Program (Grant #CD998003-09) and by Mike Ell from the North Dakota Department of Health Division of Water Quality.

References

Asrar, G., Fuchs, M., Kanemasu, E. T., & Hatfield, J. L. (1984). Estimating absorbed photosynthetic radiation and leaf area index from spectral reflectance in wheat. *Agronomy Journal*, *76*, 300−306.

Boelman, N. T., Stieglitz, M., Griffin, K. L., & Shaver, G. R. (2005). Interannual variability of NDVI in response to long-term warming and fertilization in wet sedge and tussock tundra. *Oecologia*, *143*, 588−597.

Clark, R. N. (1999). Spectroscopy of rocks and minerals, and principals of spectroscopy. In A. N. Rencz (Ed.), *Remote sensing for the earth sciences* (pp. 3−58). John Wiley and Sons.

Clark, R. N., Swayze, G. A., Livo, K. E., Kokaly, R. F., King, T. V. V., Dalton, J. B., et al. (2002). Surface reflectance calibration of terrestrial imaging spectroscopy data: A tutorial using AVIRIS. In R. O. Green (Ed.), *Proceeding of the 10th Airborne Earth Science Workshop, JPL Publication 02-1* California: Pasadena.

Cocks, T., Jenssen, R., Stewart, A., Wilson, I., & Shields, T. (1998). The HyMap airborne hyperspectral sensor: The system, calibration and performance. In M. Schaepman (Ed.), *1st EARSEL Workshop on Imaging Spectroscopy* (pp. 37−42). Swiss: Zurich.

Curran, P. J. (1983). Estimating green LAI from multispectral aerial photography. *Photogrammetric Engineering & Remote Sensing*, *49*, 1709−1720.

Curran, P. J., Dungan, J. L., Macler, B. A., Plummer, E. S., & Peterson, D. L. (1992). Reflectance spectroscopy of fresh whole leaves for the estimation of chemical concentration. *Remote Sensing of Environment*, *39*, 153−166.

Datt, B., McVicar, T. R., Van Niel, T. G., Jupp, D. L. B., & Pearlman, J. S. (2003). Preprocessing EO-1 Hyperion hyperspectral data to support the application of agricultural indexes. *IEEE Transactions on Geoscience and Remote Sensing*, *41*, 1246−1259.

Elvidge, C. D., & Chen, Z. (1995). Comparison of broad-band and narrow-band red and near-infrared vegetation indices. *Remote Sensing of Environment*, *54*, 38−48.

Enriquez, S., Duarte, C., & Sand-Jensen, K. (1993). Patterns in decomposition rates among photosynthetic organisms: The importance of detritus C:N:P content. *Oecologia*, *94*, 457−471.

Everitt, J. H., Escobar, D. E., & Richardson, A. J. (1989). Estimating grassland phytomass production with near-infrared and mid-infrared spectral variables. *Remote Sensing of Environment*, *30*, 257−261.

Frank, A. B., & Aase, J. K. (1994). Residue effects on radiometric reflectance measurements of the Northern Great Plains rangelands. *Remote Sensing of Environment*, *49*, 195−199.

Gao, X., Huete, A., Ni, W., & Miura, T. (2000). Optical biophysical relationships of vegetation spectra without background contamination. *Remote Sensing of Environment*, *74*, 609−620.

Hill, M., Donald, G. E., Hyder, M. W., & Smith, C. G. (2004). Estimation of pasture growth rate in the south west of Western Australia from AVHRR NDVI and climate data. *Remote Sensing of Environment*, *93*, 528−545.

Huang, Z., Turner, B. J., Dury, S. J., Wallis, I. R., & Foley, W. J. (2004). Estimating foliage nitrogen concentration from HyMap data using continuum removal analysis. *Remote Sensing of Environment*, *93*, 18−29.

Hunt, R. E., Jr., Everitt, J. H., Ritchie, J. C., Moran, M. S., Booth, D. T., Anderson, G. L., et al. (2003). Applications and research using remote sensing for rangeland management. *Photogrammetric Engineering & Remote Sensing*, *69*, 675−693.

Jacquemoud, S., Baret, F., Andrieu, B., Jaggard, K., & Danson, F. M. (1995). Extraction of vegetation biophysical parameters by inversion of the PROSPECT+SAIL models on sugarbeet canopy reflectance data. Application to TM and AVIRIS sensors. *Remote Sensing of Environment*, *52*, 163−172.

Kawamura, K., Akiyama, T., Yokota, H., Tsutsumi, M., Yasuda, T., Watanabe, O., et al. (2005). Quantifying grazing intensities using geographic information system and satellite remote sensing in the Xilingol steppe region, Inner Mongolia, China. *Agriculture, Ecosystems and Environment*, *107*, 83−93.

Kokaly, R. F. (2001). Investigating a physical basis for spectroscopic estimates of leaf nitrogen concentration. *Remote Sensing of Environment*, *75*, 153−161.

Kokaly, R. F., & Clark, R. N. (1999). Spectroscopic determination of leaf biochemistry using band depth analysis of absorption features and stepwise linear regression. *Remote Sensing of Environment*, *67*, 267−287.

Liang, S., Fang, H., Morisette, J. T., Chen, M., Shuey, C. J., Walthall, C. L., et al. (2002). Atmospheric correction of Landsat ETM+ land surface imagery: II Validation and applications. *IEEE Transaction on Geoscience and Remote Sensing*, *40*, 1−10.

Littell, R. C., Milliken, G. A., Stroup, W. W., & Wolfinger, R. D. (1996). *SAS system for mixed models.* Cary, NC: SAS Inst., Inc.

Loris, V., & Gianelle, D. (2006). Mapping the green herbage ratio of grassland using both aerial and satellite-derived spectral reflectance. *Agriculture, Ecosystems and Environment*, *115*, 141−149.

Matson, P. A., Johnson, L., Billow, C., Miller, J., & Pu, R. (1994). Seasonal pattern and remote spectral estimation of canopy chemistry across the Oregon transect. *Ecological Applications*, *4*, 280−298.

Moran, M. S., Inoue, Y., & Barnes, E. M. (1997). Opportunities and limitations for Image-based remote sensing in precision crop management. *Remote Sensing of Environment*, *61*, 319−346.

Mutanga, O., Skidmore, A. K., & Prins, H. H. T. (2004). Predicting in situ pasture quality in the Kruger National Park, South Africa, using continuum-removed absorption features. *Remote Sensing of Environment*, *89*, 393−408.

Myneni, R. B., Hoffman, S., Knyazikhin, Y., Privette, J. L., Glassy, J., Tian, Y., et al. (2002). Global products of vegetation leaf area and fraction absorbed PAR from year one of MODIS data. *Remote Sensing of Environment*, *83*, 214−231.

Omernik, J. M. (1987). Ecoregions of the conterminous United States. *Annals of the Association of American Geographers*, *77*, 118−125.

Phillips, R. L., Beeri, O., & DeKeyser, S. (2005). Remote wetland assessment for Missouri Coteau prairie glacial basins. *Wetlands*, *25*, 21−35.

Phillips, R. L., Beeri, O., & Liebig, M. (2006). Landscape estimation of canopy C:N ratios under variable drought stress in Northern Great Plains rangelands. *Journal of Geophysical Research*, *111*, G02015.

Roughgarden, J., Running, S., & Matson, P. A. (1991). What does remote sensing do for ecology. *Ecology*, *72*, 1918−1922.

Rundquist, B. C. (2002). The influence of canopy green vegetation fraction on spectral measurements over native tallgrass prairie. *Remote Sensing of Environment*, *81*, 129−135.

Schlerf, M., Atzberger, C., & Hill, J. (2005). Remote sensing of forest biophysical variables using Hymap imaging spectrometer data. *Remote Sensing of Environment*, *95*, 177−194.

Serrano, L., Penuelas, J., & Ustin, S. L. (2002). Remote sensing of nitrogen and lignin in Mediterranean vegetation from AVIRIS data: Decomposing biochemical from structural signals. *Remote Sensing of Environment*, *81*, 355−364.

Starks, P. J., Zhao, D., Phillips, W. A., & Coleman, S. W. (2006). Development of canopy reflectance algorithms for real-time prediction of Bermuda grass pasture biomass and nutritive values. *Crop Science*, *46*, 927−934.

Strong, L. L., Skebar, T. H., & Kermes, K. E. (2005). *North Dakota Gap analysis project.* Jamestown, ND: U.S. Geological Survey 451 pp.

Todd, S. W., & Hoffer, R. M. (1998). Responses of spectral indices to variations in vegetation cover and soil background. *Photogrammetric Engineering & Remote Sensing*, *64*, 915−921.

Tucker, C. J., Vanpreat, C., Boerwinkel, E., & Gaston, A. (1983). Satellite remote sensing of total dry matter production in the Senegalese Sahel. *Remote Sensing of Environment*, *13*, 461−474.

USDA, N. R. C. S. (2006). *The PLANT Database.*Baton Rouge, LA: National Plant Data Center (http://plants.usda.gov).

Vogelmann, J. E., Howard, S. M., Yang, L., Larson, C. R., Wylie, B. K., & Var Driel, N. (2001). Completion of the 1990s National Land Cover Dataset for the conterminous United States from Landsat Thematic Mapper data and ancillary data sources. *Photogrammetric Engineering & Remote Sensing*, *67*, 650−652.

Wessman, C. A., Aber, J. D., Peterson, D. L., & Melilllo, J. M. (1988). Remote sensing of canopy chemistry and nitrogen cycling in temperate forest ecosystem. *Nature*, *335*, 154−156.